THE ASTROPHYSICAL JOURNAL, 418:476–489, 1993 November 20

HELIOSEISMIC LINE SHAPE ESTIMATION GIVEN STOCHASTIC EXCITATION

JOHN F. KELLY AND MICHAEL H. RITZWOLLER
University of Colorado, Department of Physics, Campus Box 390, Boulder, CO 80309-0390
Received 1992 May 20; accepted 1993 May 18

ABSTRACT

Spectral parameter estimation for physical systems with complicated temporal forcing functions is poorly developed. Yet, to discern the effect of large-scale convection on helioseismic line widths (cf. Lavely & Ritzwoller; Ritzwoller & Kelly, we require a method to retrieve line shape information in the presence of a stochastic source spectrum. We consider the properties of two estimators, each designed to deal with the effects of a complicated source spectrum differently. We show that one of the estimators (eqs. [10], [20]–[24]), based on a Monte Carlo model of the source spectrum, accurately estimates input line-width and amplitude trends and their errors in an idealized, but realistic, simulation of helioseismic data. The success of this method requires its application not to individual spectral lines, but to the estimation of smooth trends over a large number of spectral lines, for example, along a helioseismic dispersion branch. On average, additive noise amplifies and broadens spectral lines and tends to mimic the line-broadening effect of convection. This biasing is shown to have a relatively small effect on the line width variation within each multiplet, but can severely bias modal average amplitude and line width. Cross talk due to incomplete spatial sampling biases line widths more significantly, but a technique exists that may correct for its most significant components. Finally, line width measurement accuracy degrades as the duration of the time series length shortens, but accurate measurements of realistic line widths can be achieved with time series lengths as short as 1 month.

Subject headings: convection — Sun: oscillations

1. INTRODUCTION

Consideration of many physical problems requires the estimation of the properties of damped harmonic resonances. Spectral analysis to estimate the small set of parameters that characterize the shapes of such resonance functions is usually applied in the frequency domain where the power spectrum of the data can frequently be related to a set of Lorentzian functions. Spectral parameters, such as line widths, amplitudes, and center frequencies, are functions of the physical system governing the spectra. Thus, spectral parameter estimates often form data in inversions for models of the underlying physical system, and their accurate and reliable estimation is the subject of much interest in many fields of geophysics and astrophysics.

The purpose of this paper is to discuss the estimation of spectral line characteristics where spectral peaks are obscured by a complicated source time function. As discussed below, this source function appears as *multiplicative noise* in the frequency domain. If it is a complicated function of frequency, it will distort the spectral line characteristics we wish to estimate. Although we attempt to present the methods discussed in this paper, as generally as possible, our motivation has been to develop methods by which helioseismic line amplitudes and widths can be estimated accurately. Consequently, our discussion will focus on the spectra of oscillating systems, and our numerical simulations will concentrate on the problem of estimating helioseismic line characteristics, in particular line widths. The motivation for our emphasis on line widths comes from Lavely & Ritzwoller (1993) who argue that large-scale nonaxisymmetric convection should affect helioseismic line widths in the systematic way that will be described below.

Although the physics governing various oscillating systems may differ, many systems share a common mathematical formulation. For example, the Earth's core nutations, seismic oscillations, oceanic internal waves, atmospheric tides, and helioseismic oscillations are all governed by equations of the form

$$\frac{\partial^2}{\partial t^2} d(r, t) + \mathcal{L}(r) d(r, t) = \sigma(r, t) , \tag{1}$$

where $d(r, t)$ is a displacement field defined over the body and $\sigma(r, t)$ repesents a forcing function. The operator $\mathcal{L}(r)$ contains the dependence on the body's internal composition and dynamics and is written here as time independent so that the equations separate. If the forcing function's time dependence can be written

$$\sigma(r, t) = \sigma(r) h(t) , \tag{2}$$

where $h(t)$ is the *source time history*, and if a solution can be found for a time-independent source, then the full solution can be written as the convolution

$$d(t) = \int_0^\infty s(t - t') h(t') dt' , \tag{3}$$

where $s(t)$ is the *natural response* of the system and solves

$$\frac{\partial^2}{\partial t^2} s(r, t) + \mathcal{L}(r) s(r, t) = \sigma(r) \delta(t) . \tag{4}$$

After Fourier transformation, the convolution in equation (3) becomes a simple pointwise multiplication:

$$d(\omega) = s(\omega) h(\omega) , \tag{5}$$

where $s(\omega)$ is the *natural spectrum* and $h(\omega)$ is the *source spectrum*. As equation (5) shows, the source spectrum acts as multiplicative noise in the frequency domain, through which we wish to retrieve the characteristics of $s(\omega)$. More complicated source functions can be represented by superposing a number of sources of the form given by equation (2), as Lavely & Ritzwoller (1992) discuss. They also argue that in helio-

seismology the average of an ensemble of many spectra, each formed with a different source spectrum, converges to the natural spectrum. Thus, the *ensemble average* of $d(\omega)$ is $s(\omega)$. Each source spectrum for a single time interval is called a *single realization* of the source process, and $d(\omega)$ is a single realization of the data spectrum.

Differences between the spectral characteristics among oscillating systems lie in the details of their dispersion relations, and in their excitation and damping. For the purposes of this paper, we assume that spectral lines are well separated in frequency so that differences in dispersion curves, though very interesting physically, can be effectively ignored. The biggest difference in spectral parameter estimation of various oscillating systems lies in the nature of the excitation process. If a system undergoes free oscillations after a delta-like source time history, much as the Earth does after a small earthquake, spectral lines are relatively uncorrupted by the excitation process, and estimation of the characteristics of the natural resonance function is straightforward (e.g., Dahlen 1979; Chao & Gilbert 1980; Masters & Gilbert 1982; Park, Lindberg & Thomson 1987; Lindberg & Park 1987; Lavely & Ritzwoller 1993). In fact, such a simple excitation process admits a deterministic estimation of the source moments (e.g., Dziewonski & Woodhouse 1983). Other systems are driven by purely periodic forces, such as the tides. These forces do obscure spectral characteristics, but in a known way, so that the corrupting effects can be corrected. The analysis of stochastically excited systems, such as helioseismic oscillations that are most likely excited by turbulent convection in the solar photosphere is more difficult. In this case, stochastic multiplicative noise obscures spectral lines and obstructs spectral line width measurement, preventing any deterministic estimation of the source process. In realistic simulations of the helioseismic source process, the shape of the resonance function can be altered severely by the source spectrum. (See Figs. 1 and 2.) As shown in Figure 3, when applied to synthetic data from these simulations, straightforward techniques for estimating resonance function parameters often return values grossly in error.

To estimate spectral parameters accurately for a physical system with a highly complicated source time history, better estimation techniques must be devised. The first criterion for a new method is to return accurately the parameters of the natural resonance function line shape beneath the multiplicative noise. The imposition of the multiplicative noise, however, inherently robs the data of information necessary to recover the underlying shape perfectly. Therefore, an equally important criterion for a new method is to provide a meaningful estimate of the errors of the spectral estimates.

We investigate the properties of two simple estimators. Let $d_{\text{model}}(\omega) = h_{\text{model}}(\omega)s_{\text{model}}(\omega)$ represent a *synthetic* or *model spectrum*. The synthetic natural resonance function, $s_{\text{model}}(\omega)$, or set of natural resonance functions can be fully represented by a set of parameters $\{c_j\}$ (defined in § 2) which we wish to estimate. The *synthetic source spectrum* is given by $h_{\text{model}}(\omega)$ and its characteristics are dependent on the nature of the source of the oscillations. Define $\Delta d(\omega) = d(\omega) - d_{\text{model}}(\omega)$ as

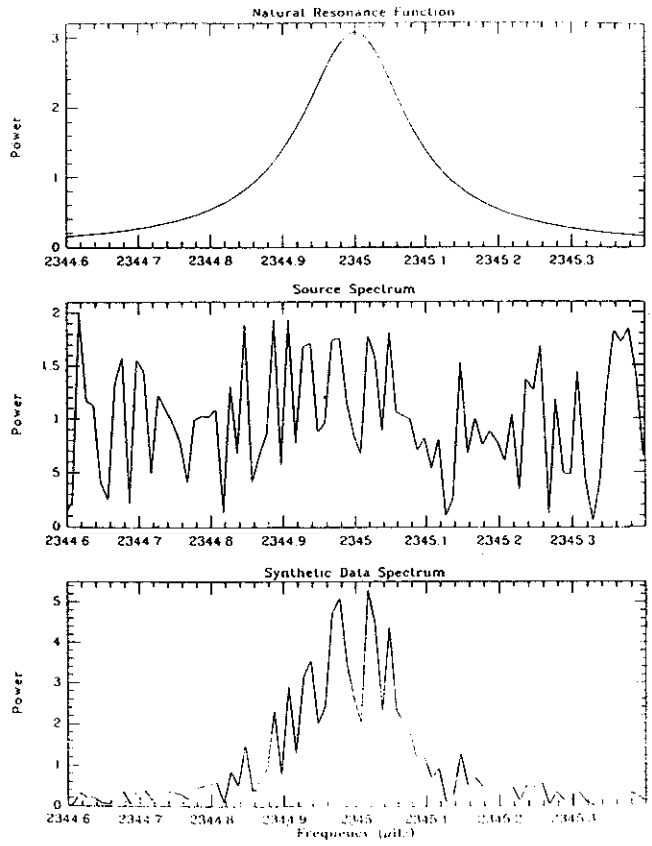

FIG. 1.—Illustration of the way in which a pure Lorentzian (*top*), $s(\omega) = \Lambda(\omega)$, is modified by a stochastic source spectrum, $h(\omega)$, represented by a noise sequence of unit expected value that is uniformly distributed in frequency (*middle*). The resultant spectrum (*bottom*), $d(\omega)$, is by eq. (5) the product of the Lorentzian and the source spectrum, which can be seen to act as multiplicative noise. The sampling rate is 0.03 μHz, but convolution with a finite time series length taper is not included.

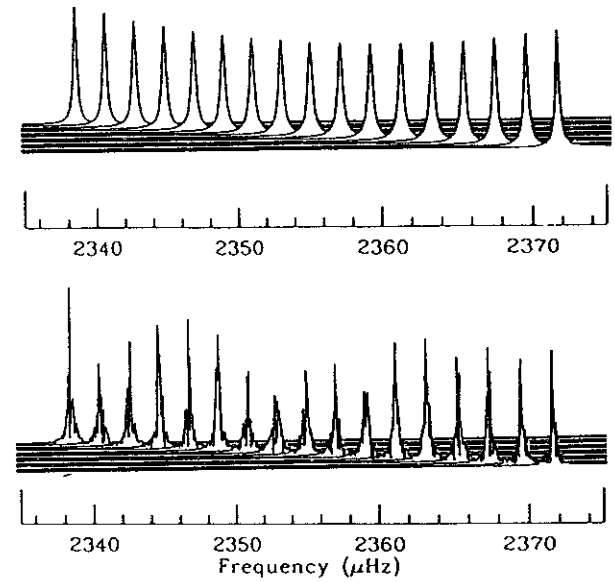

FIG. 2.—*Top:* Plot of the 17 Lorentzians that compose the multiplet ${}_3S_8$, with the azimuthal order $m = l$ singlet all the way in back, with m incremented by negative one to the $m = -l$ singlet directly in front. Amplitude and line width variations with m across the multiplet are goverend by eq. (20), where input $\{A_0, A_2, \alpha_0, \alpha_2\}$ are given in Table 1. These values are the ensemble average values for $\{A_0, A_2, \alpha_0, \alpha_2\}$ determined in Lavely & Ritzwoller (1993) from a model of giant-cell convection supplied by G. Glatzmaier for the multiplet ${}_3S_{100}$. Since the line width and amplitude contrasts within a multiplet increase with l, the use of these values for ${}_3S_8$ enhances visual variations for this plot. *Bottom:* Plot of the same 17 Lorentzians modified by a stochastic source spectrum identically as shown in Fig. 1.

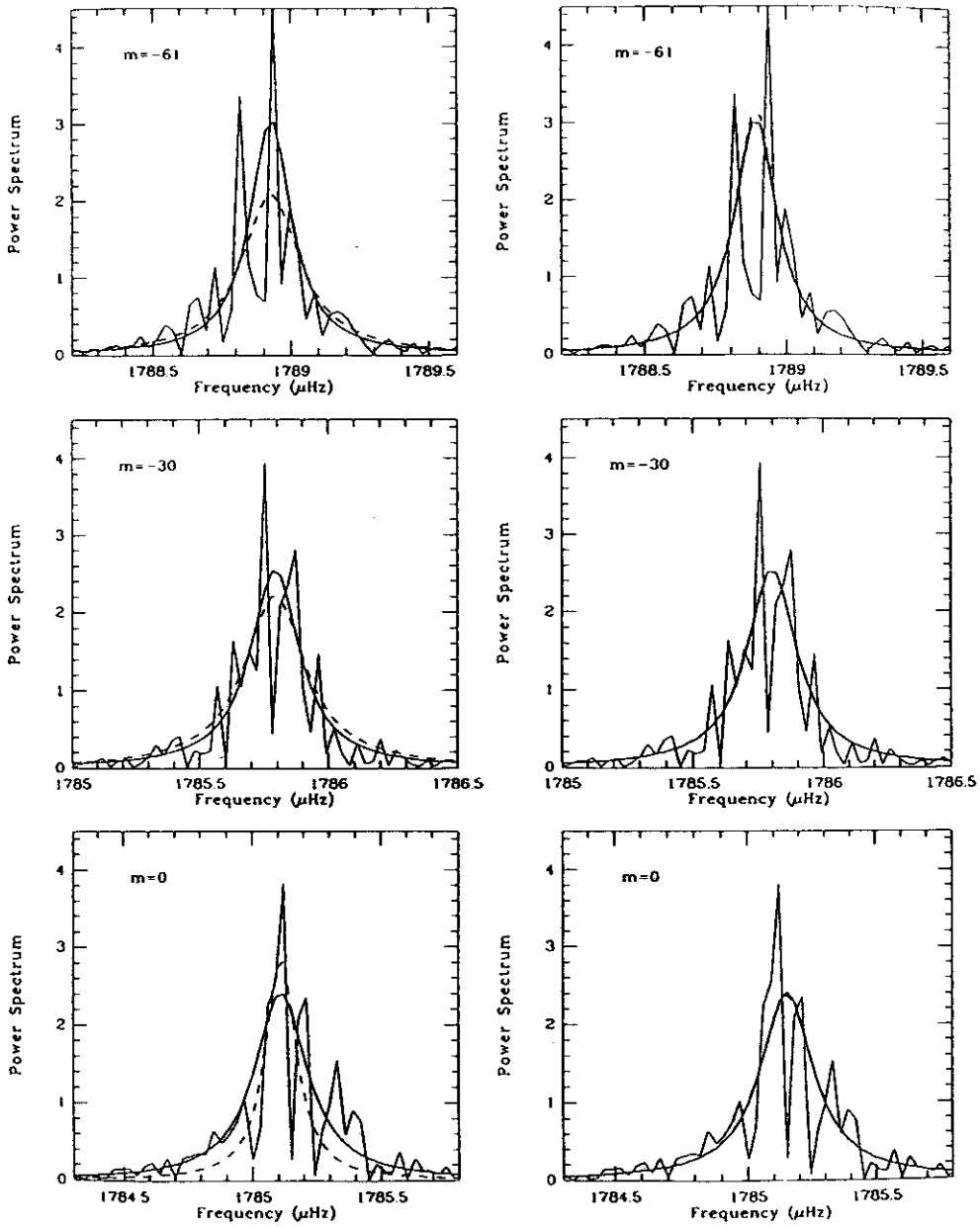

FIG. 3.—Illustration of the superiority of straight multiplet fitting over singlet fitting. *Left:* Results from singlet fitting. Plots of three Lorentzians (*thick solid line*), $\Lambda^{(m)}(\omega)$, modified by uniformly distributed multiplicative noise (*thin solid line*), $h(\omega)$, and the best fitting Lorentzian to each noisy line (*dashed line*). The multiplet is ${}_3S_{61}$ with $m = -61$ (*top*), $m = -30$ (*middle*), and $m = 0$ (*bottom*) plotted. The fit to each singlet by a single Lorentzian is systematically poor. (*Right*): Results from multiplet fitting. The legend is the same as for the left column, but here the dashed line for each m value has been estimated by fitting for the trends across the entire multiplet represented by the multiplet parameters $\{A_0, A_2, \alpha_0, \alpha_2\}$. Table 1 summarizes the fits to the amplitude and Q for each line and shows that the multiplet fitting reduces average errors by approximately an order of magnitude relative to singlet fitting.

the *residual spectrum*. We consider two 2-norm estimators that minimize the residual in a specified frequency band in two ways:

$$\min \int_{\omega_1}^{\omega_K} |\Delta d(\omega)|^2 \, d\omega \,, \tag{6}$$

$$\min \int_{\omega_1}^{\omega_K} |\Delta \ln d(\omega)|^2 \, d\omega \,, \tag{7}$$

where the absolute value symbols indicate the modulus of a complex-valued function and the minimization is over some suitably chosen frequency band $[\omega_1, \omega_K]$. The goal of each method is to represent the source spectrum accurately and to develop an error analysis for the case of multiplicative noise. The motivation for the estimator given by equation (7) is that the natural logarithm converts the multiplicative noise into additive noise, for which we can provide error estimates on the estimated coefficients.

This paper is divided as follows. In § 2 we specify the problem for helioseismic parameter estimation and present a general discussion of the two methods of spectral estimation abstractly given by equations (6) and (7). We argue that for helioseismic applications, use of estimator (6) is preferable to estimator (7), and describe a means of treating the source spec-

trum that we call Monte Carlo modeling, which when applied to coefficient estimation produces a method we call Quasi–Monte Carlo parameter estimation. This estimator is applied to idealized, but realistic, simulations of helioseismic data in § 3. In § 4, we briefly discuss the effects of additive noise, finite time series lengths, data gaps and nonuniform spatial sampling on spectral line shapes and on the retrieval of natural line shape information.

2. METHODS

The simulation of the effect of large-scale convection on helioseismic oscillations, ignoring the effects of the random source-time history, is discussed by Lavely & Ritzwoller (1992, 1993). Simulation of the source-time history will be discussed in a later contribution in which we will argue that the solar source spectrum should be stochastic and uniformly distributed in modulus and phase. These simulations are based on the currently prevailing view that helioseismic oscillations are excited by acoustic noise generated by turbulent convection near the solar surface (Goldreich & Kumar 1988; Kumar & Goldreich 1989; Brown 1990), and are in agreement with observations (Woodward 1984).

In estimating characteristics of helioseismic spectra, we are primarily interested in accurately estimating peak widths, amplitudes, and center frequencies. Since the stochastic nature of the source randomizes spectral phase information, we will ignore the phase of the spectrum.

2.1. *Spectral Estimation for a Single Resonance Function: Singlet Fitting*

Although each helioseismic spectral line is actually composed of a set of unresolved Lorentzians (Lavely & Ritzwoller, 1992, 1993), for simplicity we will approximate each peak as a single Lorentzian and will refer to it as a *singlet*. In helioseismology, each singlet can be represented by a triplet of numbers: the radial order n, and the harmonic degree l and azimuthal order m of the spatial filter. The nature of helioseismic spectral estimation for the more realistic non-Lorentzian case will be discussed in a later contribution.

Consider, first, a natural resonance function given by a single Lorentzian, $\Lambda(\omega)$:

$$s(\omega) = \Lambda(\omega) = \frac{A}{\alpha^2 + (\omega - \omega_0)^2}, \tag{8}$$

where A/α^2 is the amplitude of the spectral peak at $\omega = \omega_0$, α is the attenuation rate (which is half the line width at the half-maximum point of the amplitude spectrum), and ω_0 is the center frequency. The attenuation rate is often defined in terms of a quality factor Q by

$$\alpha = \frac{\omega}{2Q}. \tag{9}$$

In accord with equation (5), to approximate a single realization of the helioseismic spectrum we must multiply the Lorentzian by a uniformly distributed source spectrum, $h(\omega)$, as seen in Figure 1. We wish to estimate the set of *singlet parameters* $\{A, \alpha, \omega_0\}$ using the estimators defined by equations (6) and (7). This estimation procedure is called *singlet fitting*. We treat equation (6) by solving the following matrix equation iteratively, updating the singlet coefficient vector c ($c_1 = A$, $c_2 = \alpha$, $c_3 = \omega_0$) and the partial derivative matrix D on each iteration i (hereafter suppressed):

$$\Delta d^{(i)} = \mathbf{H}\mathbf{D}^{(i)}\delta c^{(i)}, \tag{10}$$

where $c^{(i)} = c^{(i-1)} + \delta c^{(i)}$ and Δd is the vector composed of the residual spectrum arrayed row-wise as a function of frequency ω_j:

$$\Delta d(\omega_j) = d(\omega_j) - \Lambda(w_j)h_{\text{model}}(\omega_j). \tag{11}$$

the matrix $\mathbf{H}$ is the diagonal matrix whose nonzero elements are the estimates of the source spectrum: $H_{kk'} = h_{\text{model}}(\omega_k)\delta_{kk'}$. The model spectrum chosen can be any member of an ensemble of spectra that have a prescribed distribution function with respect to source amplitude. [See § 2.3 for a more detailed discussion of $h_{\text{model}}(\omega_k)$.] The frequency band over which fitting is performed is discrete with $\omega_k \in [\omega_1, \ldots, \omega_K]$. The $K \times 3$ partial derivative matrix is given by

$$D_{k1} = \frac{\partial \Lambda(\omega_k)}{\partial A} = \frac{1}{A}\Lambda(\omega_k), \tag{12}$$

$$D_{k2} = \frac{\partial \Lambda(\omega_k)}{\partial \alpha} = \frac{-2\alpha}{A}\Lambda^2(\omega_k), \tag{13}$$

$$D_{k3} = \frac{\partial \Lambda(\omega_k)}{\partial \omega_0} = \frac{2(\omega_k - \omega_0)}{A}\Lambda^2(\omega_k). \tag{14}$$

Similarly, we treat equation (7) by iteratively solving

$$\Delta \ln d^{(i)} = P^{(i)}\delta c^{(i)}, \tag{15}$$

where the partial derivative matrix P is given by

$$P_{kj} = \frac{\partial \ln [\Lambda(\omega_k)]}{\partial c_j} = \frac{D_{kj}}{\Lambda(\omega_k)}. \tag{16}$$

The residual of the logarithm is defined as follows:

$$\begin{aligned}\Delta \ln d(\omega) &= \ln d(\omega) - \ln d_{\text{model}}(\omega) \\ &= [\ln s(\omega) + \ln h(\omega)] - [\ln \Lambda(\omega) + \ln h_{\text{model}}(\omega)] \qquad (17) \\ &= \Delta \ln s(\omega) - [\ln h_{\text{model}}(\omega) - \ln h(\omega)] \\ &= \Delta \ln s(\omega) - n(\omega), \qquad (18)\end{aligned}$$

which allows us to rewrite equation (15) as

$$\Delta \ln s^{(i)} = P^{(i)}\delta c^{(i)} + n, \tag{19}$$

where $n_k = [\ln h_{\text{model}}(\omega_k) - \ln h(\omega_k)]$ is the difference between the actual source spectrum and our model source spectrum and can be considered to be additive noise. Its statistics will depend on the nature of the source process. For helioseismic spectra, it should be log uniform. Taking the logarithm transforms the multiplicative noise into additive noise, from which error estimates are easily computed.

Thus, we implement the estimators given by equations (6) and (7) by solving equations (10) and (19) and refer to these methods as *straight and logarithmic fitting*, respectively. Unfortunately, simulations indicate that in the presence of a uniformly distributed source spectrum neither estimator retrieves the input amplitudes and line widths accurately. Figure 3 and Table 1 show that the multiplicative noise produces a spectrum that is poorly fitted by a Lorentzian, and the estimated spectral line parameters differ markedly from the input parameters. Unless an accurate, deterministic estimate of the source spectrum exists, the estimates of line width and amplitude will contain large errors. Frequency estimates are not similarly biased. Multiplicative noise does increase their variance, but frequencies can even be well estimated by the moment-ratio

TABLE 1

SUMMARY OF THE FITTED AMPLITUDES AND Qs IN FIGURE 3

m	A_m	Error (%)	Q_m	Error (%)
Input Values				
−61	1.005	...	9821	
−30	1.249	...	8257	
0	1.490	...	7139	
Multiplet Fit				
−61	1.033	1.0	9862	0.4
−30	1.299	4.0	8110	1.8
0	1.563	4.9	6904	3.3
Singlet Fit				
−61	1.350	34	6991	29
−30	1.861	49	6123	26
0	0.579	61	12542	76

Computed values of resonance peak amplitude and quality factor for three different azimuthal orders m of the multiplet ${}_3S_{61}$. The singlet and multiplet fitting routines were supplied with an identical full multiplet data set of pure Lorentzian functions to which uniformly distributed multiplicative noise had been applied. The line widths and amplitudes of each singlet were computed from the line width trend parameters $\{A_0, A_2, \alpha_0, \alpha_2\}$ computed in Lavely & Ritzwoller 1993. These input values are listed for $m = -61$, $m = -30$, and $m = 0$. The line shape corruption due to the application of multiplicative noise substantially biases the singlet parameter estimates, yielding estimates with errors of $\sim 50\%$. This biasing error is greatly diminished if line width trends are sought by simultaneously fitting over the entire multiplet (see Fig. 3.)

method (e.g., Lavely & Ritzwoller 1993). Since frequency estimation is not problematic, we will drop discussion of it hereafter. Experience shows that what is needed to estimate spectral line widths and amplitudes accurately is to consider not a single spectral line, but variations in line attributes across a number of lines.

2.2. *Spectral Estimation over Multiple Resonance Functions: Multiplet Fitting*

Information is lost from the spectrum when multiplicative noise is applied to the underlying resonance function. To retrieve this information requires the addition of auxillary information. For helioseismology, this information is that, irrespective of multiplicative noise, helioseismic spectral characteristics are expected to vary smoothly and slowly within a multiplet and therefore variations can be parameterized in terms of simple functions. Lavely & Ritzwoller (1993) showed that certain models of large-scale convection in the solar interior possess an amplitude and line width signature in helioseismic data which, to a good approximation, can be modeled by a degree two polynomial in m/l. They also showed that the polynomial coefficients should trend approximately linearly with harmonic degree l. Optimally, line widths and amplitudes should be parameterized simply in terms of the n of each node and the l and m of the spatial filter, and the spectra of all the lines should be fitted simultaneously. The simulations reported in § 3 show that it is sufficient to estimate the amplitude and line width variations within a single multiplet and then fit a posteriori for trends with l and n. (A *multiplet* comprises the $(2l + 1)$ lines, each characterized by a different m, for a single n and l.)

We call this fitting for the amplitude and line width trends within a multiplet, *multiplet fitting*. Like singlet fitting, multiplet fitting is based on equations (10) and (19), but with the following transformations: $\Lambda(\omega_k) \rightarrow \Lambda^{(m)}(\omega_k)$, $D \rightarrow \tilde{D}$, and $P \rightarrow \tilde{P}$, where the features of the Lorentzians within each multiplet are given by the following equation:

$$\Lambda^{(m)}(\omega) = \frac{A_0 + A_2 P_2(m/l)}{(\omega - \omega_m)^2 + [\alpha_0 + \alpha_2 P_2(m/l)]^2} . \tag{20}$$

We wish to estimate the set of *multiple parameters* $\{c_1 = A_0, c_2 = A_2, c_3 = \alpha_0, c_4 = \alpha_2\}$ for each multiplet. Spectra in the data vector and partial derivative matrices are stacked vertically first as a function of frequency around each of the $(2l + 1)$ lines within a multiplet and then as a function of azimuthal order m so that the row index is $n = K(m + l) + k$. The $K(2l + 1) \times 4$ partial derivative matrix is given by

$$\tilde{D}_{n1} = \frac{\partial \Lambda^{(m)}(\omega_k)}{\partial A_0} = D_{k1}^{(m)} , \tag{21}$$

$$\tilde{D}_{n2} = \frac{\partial \Lambda^{(m)}(\omega_k)}{\partial A_2} = D_{k1}^{(m)} P_2(m/l) , \tag{22}$$

$$\tilde{D}_{n3} = \frac{\partial \Lambda^{(m)}(\omega_k)}{\partial \alpha_0} = D_{k2}^{(m)} , \tag{23}$$

$$\tilde{D}_{n4} = \frac{\partial \Lambda^{(m)}(\omega_k)}{\partial \alpha_2} = D_{k2}^{(m)} P_2(m/l) , \tag{24}$$

$$\tilde{P}_{nj} = \frac{\partial \ln [\Lambda^{(m)}(\omega_k)]}{\partial c_j} = \frac{\tilde{D}_{nj}}{\Lambda^{(m)}(\omega_k)} . \tag{25}$$

Although the frequencies around each line are labeled identically (ω_k), they will differ from line to line, though their number around each line will remain approximately fixed, being governed by the time series length.

Figure 3 and Table 1 show that straight multiplet fitting greatly improves the ability to retrieve natural resonance function characteristics for spectral lines within a multiplet, with errors reduced from straight singlet fitting by an l-dependent amount, approximately an order of magnitude for $l \simeq 50$.

The application of the equations (10), (19), and (20)–(25) suffers from three main problems. First, we require a model of the source spectrum, $h_{\text{model}}(\omega)$. We will discuss this in § 2.3. Second, error estimates of the estimated parameters are necessary to interpret the results. In principle, since the multiplicative noise has been transformed into additive noise by the logarithm, error estimates for the logarithmic estimator (eq. [19]) are straightforward. Unfortunately, simulations show that they are difficult to interpret since they are log-uniform in distribution. Error estimates for the straight estimator (eq. [10]) will also be discussed in § 2.3 and 3. Finally, the combined effect of additive noise and multiplicative noise has not been considered in the equations above. The logarithmic estimator is unstable to the addition of additive noise to the spectrum because the logarithm weights up the low-amplitude parts of the spectrum. When noise is added, it is preferentially fitted by the logarithmic estimator so that even very high signal-to-noise ratio data are irretrievably corrupted. This consideration causes us to discard at this point the logarithmic estimator which can perform well only in an extremely low additive-noise environment. Hereafter, only the straight estimator will be considered. The effect of additive noise on straight multiplet fitting will be discussed in § 4.

2.3. *Monte Carlo Model of the Source Spectrum and Error Estimation*

Since we cannot produce an accurate model of the stochastic solar source process to generate a model of the source spec-

trum, we choose instead to generate these spectra so as to have the same statistical characteristics as are seen in the data. To do this, we can use equation (10) iteratively to find the least-squares fit Lorentzian to the data. We then use this Lorentzian and the data to solve for $h_{\text{model}}(\omega)$ by setting the left-hand side of equation (10) to zero. By analyzing histograms of the amplitudes of $h_{\text{model}}(\omega)$, we can determine empirically its distribution function. When this technique is applied to data collected by T. Brown in 1989, we find that the distribution of source spectrum noise can be acceptably modeled as uniform.

Consider an ensemble of model source spectra distributed identically with that derived from the data, $\{h^{(p)}_{\text{model}}(\omega_k)\}^{\infty}_{p=1}$, with each member considered to be a potential single realization of the source process. We draw for this ensemble a finite number of realizations, $\{h^{(p)}_{\text{model}}(\omega_k)\}^{P}_{p=1}$. We refer to this process as a *Monte Carlo model of the source spectrum*. With each realization of the source spectrum, we solve equation (10) iteratively, yielding coefficient estimates $c^{(p)}$, and then consider the average, $\hat{c}$, and the standard deviation, $\hat{\sigma}$, of the coefficients over this ensemble of P estimates. The source process is treated statistically, but for each realization of the source spectrum, coefficient estimation is deterministic. For this reason, we refer to this process as *quasi–Monte Carlo spectral parameter estimation* or *fitting*. At the very least, in each realization, the model spectrum and the partial derivative matrix match the data statistically.

The sum of uniformly distributed functions goes to a constant function as the index on the sum increases. The average source spectrum, therefore, is a constant function of frequency, $h_{\text{model}}(\omega) = 1$ or $\mathbf{H} = \mathbf{I}$, where $\mathbf{I}$ is the identity matrix. With this model of the source spectrum, a pure Lorentzian is fitted to the data, returning limiting case coefficient estimates $\hat{c}$. We call this *Lorentzian fitting*. The nuances of individual source distributions will cause single realization coefficient estimates to differ from the Lorentzian fit estimates. As more relevant data points are considered, either by improving resolution or by fitting multiplets rather than singlets, single realization estimates converge to the Lorentzian estimates. In addition, we have found that the average of many individual realization estimates also converges to the Lorentzian estimate, as the number of instances of source spectra considered becomes large.

In § 3 we discuss the characteristics of the application of straight multiplet fitting (eqs. [10], [20]–[24]) with the Monte Carlo model of the source spectrum. We show that the expected value of the quasi–Monte Carlo coefficient estimates, $\hat{c}$, are on average accurate and converge to Lorentzian spectral estimates. In addition, we show that the standard deviation of the ensemble for each coefficient, $\hat{\sigma}$, provides a useful measure of the expected error. Although these methods are applied here only in search of the line width broadening signal predicted by Lavely & Ritzwoller (1992), the methods are a generally applicable means of measuring spectral parameter trends and their associated uncertainites. These methods may prove to be useful for measurement of frequency splitting trends used, for example, by Goode et al. (1991) to detect latitudinal and radial variations in the solar rotation rate.

3. APPLICATION TO SIMULATED HELIOSEISMIC DATA

3.1. *Synthetic Spectra*

Lavely & Ritzwoller (1993) argue that helioseismic spectral peak widths reveal more information about solar convection than other spectral parameters. They show that helioseismic spectra produced from spatially filtered images corresponding to spherical harmonic degree and order l and m, respectively, are systematically broadened for low $|m|/l$ relative to high $|m|/l$. The broadening is not an intrinsic damping effect and can be explained simply. Let $\tilde{m}$ and $\tilde{l}$ represent the azimuthal order and harmonic degree of the eigenfunctions of the spherically symmetric reference solar model. These parameters are two modal quantum numbers, unlike m and l which are two indices of a spherical harmonic spatial filter. The line broadening predicted by Lavely & Ritzwoller (1993) results from the fact that low $|\tilde{m}|/\tilde{l}$ modes tend to couple more strongly than high $|\tilde{m}|/\tilde{l}$ modes. This is because differential rotation dominates the frequency splitting and spaces low $|\tilde{m}|/\tilde{l}$ modes more closely than high $|\tilde{m}|/\tilde{l}$ modes. This coupling means that low $|m|/l$ spectra are not pure Lorentzians, but are composed of a set of unresolved spectral peaks. Using Glatzmaier's model of stationary convection (Gilman & Glatzmaier 1981; Glatzmaier & Gilman 1981, 1982; Glatzmaier 1984; Gilman & Miller 1986), Lavely & Ritzwoller (1993) show that the trend of peak widths within a multiplet is approximately parabolic in $|m|/l$. It is this peak-broadening signal, which is the signature of large-scale convection in the natural resonance functions, that we wish to estimate through the random solar source spectrum. Analysis of 1989 data observed by T. Brown indicates that such a line-broadening signal exists (Ritzwoller & Kelly 1993), but it is not yet clear that this broadening exceeds similar broadening caused by the cross talk and additive noise effects discussed in § 4.

We construct synthetic spectra along the $n = 3$ branch with l ranging from 1 to 100. For each singlet, a uniformly distributed source spectrum, $h(\omega)$, with unit expected value is applied to each natural resonance function which here is a Lorentzian. The input line shape multiplet parameters $\{A_0, A_2, \alpha_0, \alpha_2\}$ are the ensemble average estimates of Lavely & Ritzwoller (1993). Input frequencies are also taken from Lavely & Ritzwoller (1993). Our synthetic spectra here contain no "cross talk" which would be caused by the incomplete sampling of the spatial filter, nor any additive noise. Intrinsic Q is set for each mode at 10,000. This is a realistic intrinsic Q at very low frequencies, but is a factor of 3–5 too large for frequencies above 2 mHz. The frequency sampling is chosen to be 0.03 μHz, which corresponds to a time series length of roughly a year. Spectra have not been smoothed by convolution with a finite time series length nor a day–night duty-cycle function. These effects will be discussed in § 4 as well. Fitting is performed over a symmetric frequency band centered about each line down to 20% of the peak power.

3.2. *Estimation of Spectral Trends within and across Multiplets*

Each multiplet is initially considered independently, and straight quasi-Monte Carlo multiplet fitting is applied to yield estimates of the multiplet parameters $\{A_0, A_2, \alpha_0, \alpha_2\}$. Input multiplet parameters must be determined to initiate iteration. This is done in the following way. Each singlet frequency is estimated with the moment-ratio method which proves to yield a highly accurate frequency estimate. Straight singlet fitting is then applied to each singlet to determine α_m and A_m, approximately, and $\{A_0, A_2, \alpha_0, \alpha_2\}$ are initially estimated from the singlet estimates by regressing over m. A set of synthetic source spectra, $\{h^{(p)}_{\text{model}}(\omega)\}^{P}_{p=1}$, are then computed with the initial multiplet parameter estimates with statistics matching the source spectrum of the data, and straight multiplet fitting is applied iteratively to each using eqs. [10], [20]–[24]. The

numerical stability of the partial derivative matrix is quite good with typical condition numbers ~ 10, and convergence is achieved within a few iterations for each synthetic source spectrum. The averages and standard deviations of the multiplet spectral parameters taken over the P realizations of the model source spectrum are then tabulated.

Figure 4 shows the results of quasi–Monte Carlo multiplet fitting for ${}_3S_{61}$ for a single input source spectrum. (We use hereafter the geoseismologic notation ${}_nS_l$ to denote the overtone with radial order n of the spheroidal mode of oscillation with harmonic degree l.) The input values for the multiplet parameters are at the intersection of the bold crosshairs on each plot. Each small x represents the estimated multiplet parameters for a single synthetic source spectrum. The average of the estimated parameters, which is the quasi–Monte Carlo estimate, is represented by the triangle at the intersection of each error bar whose length is equal to the standard deviation of each estimated parameter. The convoluted line shows the convergence trajectory over realizations of the source spectrum. We wish to draw two conclusions from this figure. (1) As asserted in § 2.3, the quasi–Monte Carlo estimate converges to the Lorentzian fitting estimate which is represented by the small circle near the intersection of each pair of error bars. (2) The error bars can be seen to provide meaningful estimates of the errors in the estimated parameters.

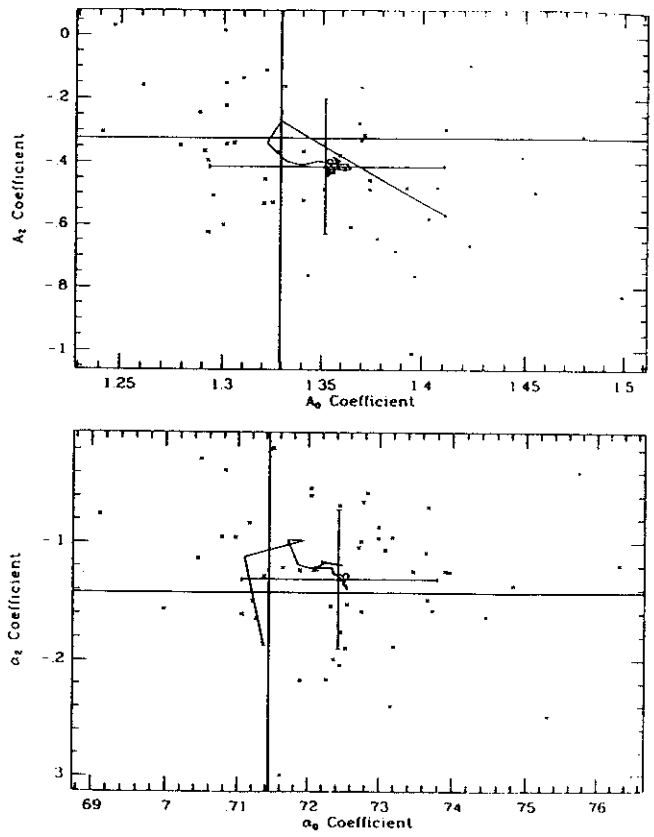

FIG. 4.—Result of straight multiplet fitting for the multiplet ${}_3S_{61}$. The bold crosshairs in each plot represent the input values for A_0, A_2, α_0, and α_2. Each small x marks the value of the pair $\{A_0, A_2\}$ and $\{\alpha_0, \alpha_2\}$ on the top and bottom panel, respectively, for a single draw of the source spectrum, $h_{model}(\omega)$. The average of this ensemble is plotted at the intersection of the error bars, which themselves represent the standard deviation of each parameter. The trajectory of the running average for each parameter is shown as the convoluted line converging on the intersection of the error bars. The small circle near the intersection of the error bars is the coefficients estimated with Lorentzian fitting, to which the quasi Monte Carlo estimates would converge as $P \to \infty$. The error bars can be seen here and in Fig. 6 to be a useful estimate of the errors in the estimated parameters.

With only a single realization of the input source spectrum for a multiplet, the quasi–Monte Carlo estimator is biased; i.e., the cloud of individual estimates seen in Figure 4 does not center on the input parameters. This arises because multiplicative noise inherently robs the spectrum of information, and changes the apparent line width and amplitude of each line. Imagine the improbable situation in which the source spectrum for a single line were zero everywhere except at the spectral peak. We could never retrieve the natural line width of this spectrum. The quasi–Monte Carlo technique assumes that we draw a "typical" synthetic source spectrum. Since in this worst case scenario the source spectrum is not typical, the estimated coefficient will be biased. For the quasi–Monte Carlo technique to reduce the bias, we must ensure that the data source spectrum is more nearly average. This can be achieved by considering not a single multiplet at a time, but a large set of multiplets. Considering a large number of lines reduces the chance that the data source spectrum is grossly atypical. This is consistent with the assertion that biases decrease with increasing l. (The number of lines over which the fit is performed increases linearly with l.) In addition, simulations show that when an improbable input source spectrum leads to large biases, the cloud coefficient estimates will have a similarly high standard deviation. We can thus use these standard deviations as a reliable estimate of the error on the estimated parameters.

Thus, application of straight quasi–Monte Carlo multiplet fitting is insufficient to retrieve accurate line shape parameters for a single multiplet. However, error estimates from this technique are meaningful and it is necessary to consider trends in the estimated parameters with l to retrieve the input values accurately. In addition, as Figure 5 shows, for each multiplet there is a high covariance between a subset of the multiplet parameters. This trade-off is also diminished by considering along-branch trends.

Figure 6 shows the results of the application of straight quasi–Monte Carlo multiplet fitting along the ${}_3S$ branch for l ranging from 40 to 100. The dark solid line represents the input values of the multiplet parameters, and the straight line is the weighted linear fit to the parameter estimates and estimated errors. We draw two conclusions from this figure. (1) Although the error for a single multiplet can be large, the fit with l accurately retrieves the input parameters. (2) The error bars approximate 1 σ errors. In each plot, approximately two-thirds of the error bars cross the input line, and the estimated errors, on average, increase with the size of the error. For example, the error and the error bars decrease with l.

In conclusion, straight quasi–Monte Carlo multiplet fitting is adequate to retrieve the along-branch trends which should be the signature of large-scale convection. As witnessed by the fact that errors decrease dramatically with l, straight quasi–Monte Carlo along-branch fitting or a similar simultaneous fitting of many neighboring multiplets would be preferable to simple multiplet fitting, although it would be much more computationally costly.

4. OTHER EFFECTS

Although the primary purpose of this paper is to describe a method by which natural line shape information can be recovered in the presence of multiplicative noise caused by a stochastic source process, there are other phenomena affecting

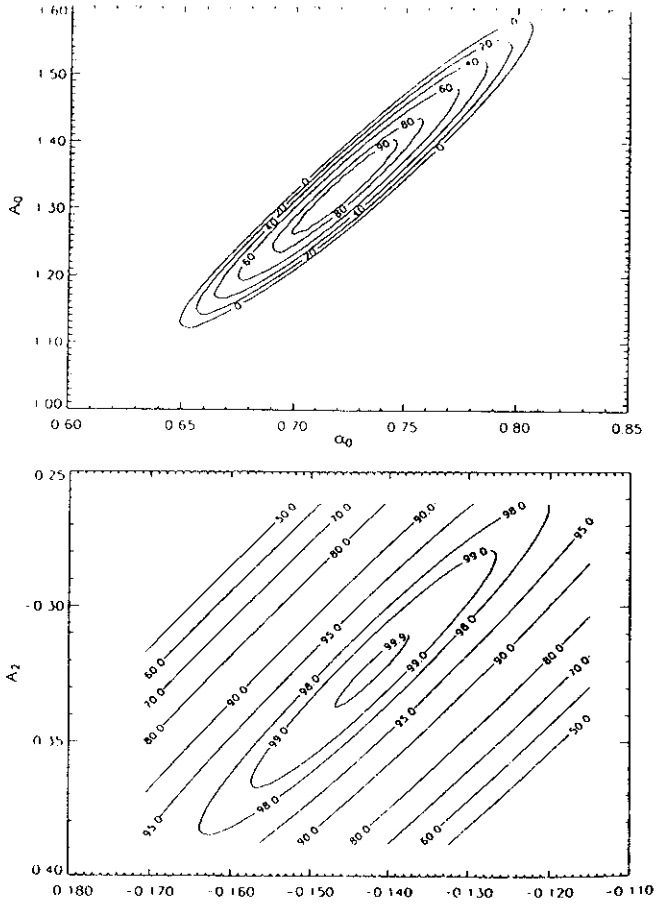

FIG. 5.—Misfit plots with contours of constant variance reduction in percent for a pure Lorentzian for ${}_3S_{61}$. Variance reduction is defined as follows: $100[1 - \{\Sigma_k[\Lambda_{\text{input}}(\omega_k) - \Lambda_{xy}(\omega_k)]^2/\Sigma_k \Lambda^2_{\text{avg}}(\omega_k)\}]$, where Λ_{input} is the input pure Lorentzian, Λ_{xy} is the Lorentzian with the (x, y) value at the point given on the plot, and Λ_{avg} is the fiducial Lorentzian with line shape parameters which are the average over all the singlets in the multiplet. Since misfit and covariance are related, strong covariance between A_0 and α_0, and A_2 and α_2 are revealed, and since variations in A_2 and α_2 produce smaller effects on the data than A_0, their relative errors will be larger.

helioseismic data that can mask the line shape signature of convection. These include additive noise (caused principally by photospheric convection), finite-gapped observing intervals, and cross talk due to nonuniform spatial sampling. To this point, our reported simulations have been additive noise-free and, although finitely sampled in the frequency domain, have been for natural resonance functions unbroadened by finite temporal observing intervals or spatial cross talk. It is important to determine the effect of additive noise, in particular on line width measurements, to place a lower bound on the time series lengths required to retrieve accurate line shape estimates and to determine the magnitude of the line width corruption caused by cross talk.

4.1. *Finite Time Series Lengths and Day–Night Gaps*

Finite time series lengths and time series gaps present no formal problem. To incorporate these effects we define a temporal sampling function (TSF) spectrum, the Fourier transform of the temporal sampling function in the time domain, which we convolve with the data spectrum, the synthetic spectrum, and the partial derivative matrix in the methods described in § 2. In practice, however, short time series lengths can smooth the data spectra to the point that line width information is irrecoverable. Figure 7 shows spectra of three TSFs, two of which are ungapped with lengths of 3 and 12 months, respectively, and one of which is gapped with a total length of 12 months. In this range of frequency offsets, the gapped and ungapped spectra nearly overlay one another, and are very difficult to resolve. Let us define the *half-width of the TSF spectrum* as the distance to the first node off the central lobe, i.e., the Fourier bin spacing. Synthetic experiments suggest that as long as the half-width of the TSF spectrum is less than half of the line width (α), then the multiplet trend parameters can be estimated accurately.

At 3 mHz, for a spectral line with $Q = 3000$, line widths at the amplitude half-maximum point are approximately $\alpha = \omega/2Q = 0.50$ μHz. The requirement that the half-width of the TSF spectrum be less than half the line width means that time series lengths should exceed ~ 20 days.

Matters worsened only slightly when time series gaps are introduced. Figure 7 shows that the amplitude spectrum for a year-long 42% duty cycle (approximately 10 hr on and 14 hr off) TSF roughly overlays the ungapped year-long TSF spectrum for small-frequency offsets. However, the 42% and the ungapped TSF spectra diverge for larger offsets as can be seen in Figure 8. The 42% duty-cycle TSF spectrum has large side peaks spaced at frequency offsets of $n/24h$ with amplitudes in excess of 70% of the central lobe amplitude. This is a serious spectral leakage problem and underscores the need for the use of Global Oscillations Network Group (GONG) data which should have a duty-cycle in excess of 90% when fully deployed (Anderson 1992). However, simulations show that this phenomenon has little systematic effect on line widths. It is the structure of the TSF spectrum for small frequency offsets which is of greatest significance.

4.2. *Additive Noise*

The effects of additive noise on the estimated multiplet parameters depend strongly on the way in which it is incorporated in the spectrum. In particular, they depend on the relative noise-to-signal ratio (NSR) as a function of m. We assume here that the absolute noise level is constant across m. Since low $|m|/l$ lines have lower amplitude in our simulations than high $|m|/l$, the relative NSR is higher for low $|m|/l$ and, therefore, the relative effect of noise is greater for low $|m|/l$. For real data, the variation in absolute noise level across m depends dominantly on the nature of the spatial filter which dictates the spatial sampling. Noise will be lowest for those spatial filters that weight the center of the observing disk the highest.

Figure 9 demostrates the way in which we add noise to power spectra. Although the stochastic nature of the source process requires us to ignore the phase of the amplitude spectrum, we cannot ignore its phase relative to the additive noise spectrum. Thus, the resultant noisy data depend on two random variables: an additive noise amplitude, $\langle N \rangle$, with a Gaussian distribution, and a uniformly distributed relative phase, ϕ, between the natural resonance function signal and the additive noise. Inspection of Figure 9 reveals that, on average, the spectral power is increased by additive noise.

We report here the result of varying the NSR on the multiplet line shape parameters. If the NSR is small, the expected value of the signal is only slightly changed; whereas if the noise and signal levels are comparable, the measured signal level is appreciably increased. Since the low $|m|/l$ lines have a smaller signal amplitude than the high $|m|/l$ lines, they have a higher

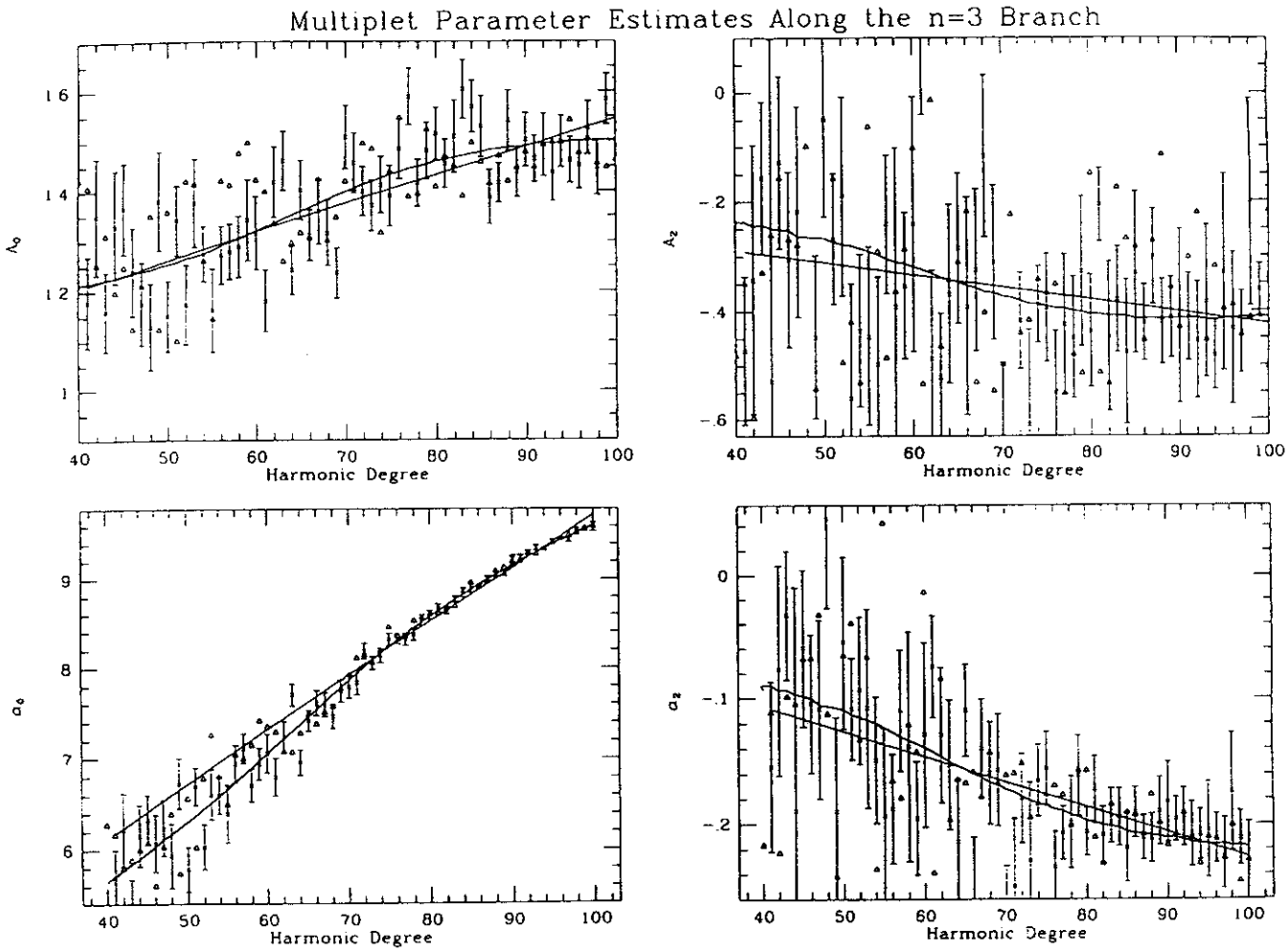

FIG. 6.—Summary of the attempt to retrieve along-branch line shape trends. In each plot, the solid line represents the input value of the specified parameter as a function of harmonic degree l. Each 1 σ error estimated by Monte Carlo source simulation is shown as an error bar with an x at the center representing the straight quasi-Monte Carlo parameter estimate. The triangles represent the values obtained from the logarithmic fit. No useful error estimates were obtained with this method and it is not suggested as a useful technique. The straight line is the best weighted linear fit to quasi-Monte Carlo estimates and shows that the along-branch trends, which should be the helioseismic signature of large-scale convection, can be retrieved accurately.

NSR on average. Although additive noise raises the observed power level of all lines, it has a larger relative effect on low $|m|/l$ lines and therefore, tends to diminish the amplitude contrast between lines within a multiplet. In addition, additive noise broadens spectral lines. This broadening is relatively greater for narrow lines than for broad lines, so that it has a larger effect, on average, on high $|m|/l$ lines than on low $|m|/l$ lines. Thus, additive noise has a complementary effect on peak amplitudes and line widths. Recall that peak amplitudes here equal A/α^2, which implies that the effect of additive noise on modal line widths and amplitudes will be the result of this competition. Figure 10 displays the measured values of the singlet amplitude A and attenuation α parameters and shows that, on average, the α effect dominates. Thus additive noise tends to broaden low $|m|/l$ lines in relation to high $|m|/l$ lines, which mimics the multiplet trend due to large-scale convection in both the amplitude and attenuation parameters.

Figure 10 shows that the effect on the multiplet parameters by additive noise actually peaks at mid-range $|m|/l$ values, but displays nearly a parabolic shape in m. In fact, the effect of additive noise can be represented by a simple transfer function in m, relating the input (A, α) to the estimated $(\hat{A}, \hat{\alpha})$ values:

$$\hat{A}_m = T_A(m)A_m , \tag{26}$$

$$\hat{\alpha}_m = T_\alpha(m)\alpha_m . \tag{27}$$

These transfer functions are dependent on the NSR and on the input values of the multiplet parameters, and thus removing the effects of additive noise by inverting equations (26)–(27) could be a difficult transcendental problem. This difficulty is mitigated for two reasons: the correction is small for the parameters of greatest interest, and the dependence of the transfer function on additive noise level is much stronger than its dependence on the values of the input parameters. Since the spectral parameter of greatest interest is the line width α, $T_\alpha(m)$ is the most important function to invert. Figure 11*b* shows that for a representative value of 4% additive noise in the power spectrum, $T_\alpha(m)$ is less than 10% different from unity. Thus, the bias due to additive noise will be small in comparison to other biases to which line width measurements are subject. Figure 11 also shows that variations in the additive noise levels produce much bigger changes in the transfer functions than do varia-

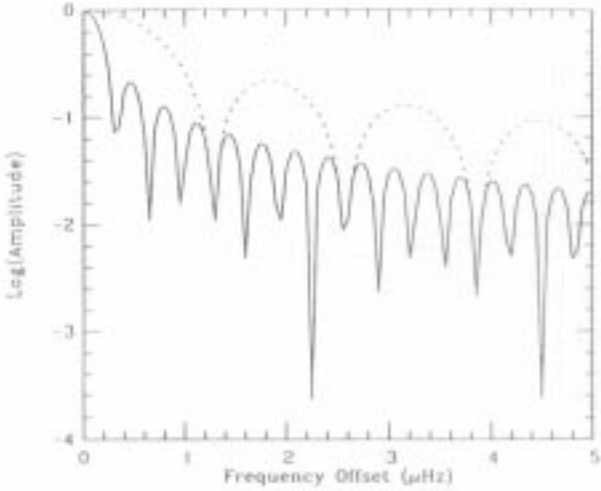

FIG. 7.—Amplitude spectra for three different temporal sampling functions (TSF). *Dashed line:* 3 month ungapped time series; *solid line:* 1 yr ungapped time series; *dotted line:* Year-long time series with a 42% duty cycle, 10 hr on and 14 hr off each day. The solid and dotted lines approximately overplot at the small frequency offsets shown here. The half-width of each TSF spectrum is defined as the distance to the first spectral node off the central lobe, i.e., the Fourier bin spacing.

tions in input parameters. This suggests that as a first approximation, the transfer function might be considered to be only a function of additive noise level. Inversion of equations (26)–(27) is then simple division. Note that this approximation improves as additive noise level increases.

The effect of varying the NSR on the estimated multiplet coefficients is shown in Figure 12. Clearly, the multiplet trend parameters (A_2, α_2) are affected less severely by additive noise

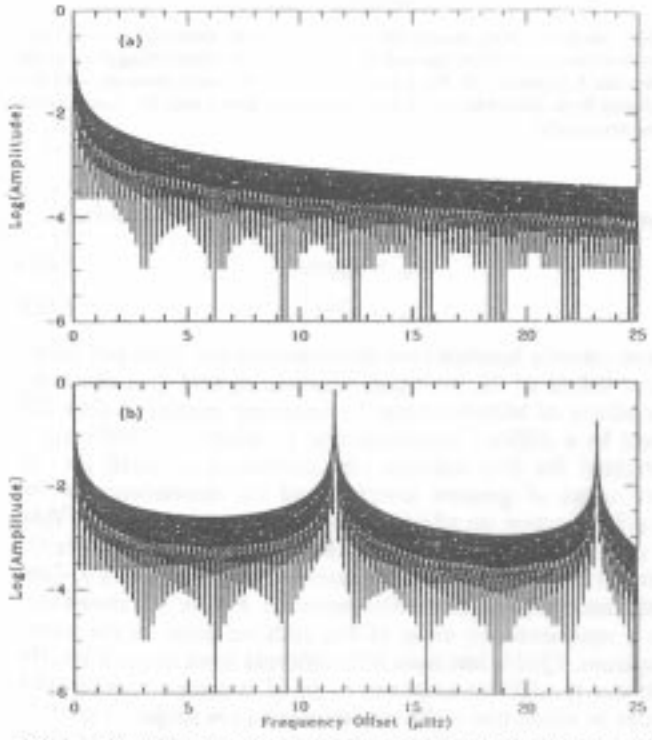

FIG. 8.—(*a*) Amplitude spectrum of a year-long ungapped time series. (*b*) Amplitude spectrum of the year-long temporal sampling function with a 42% duty cycle.

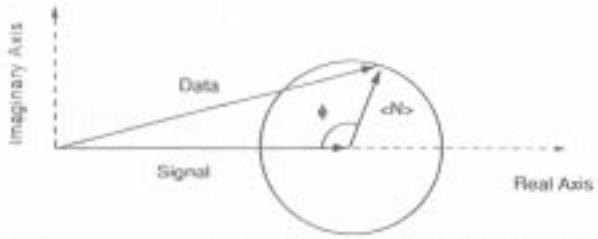

FIG. 9.—Way in which noise is added to power spectra for synthetic experiments with additive noise. Although the natural resonance functions have zero-phase, noise is represented by its expected values, $\langle N \rangle$, which has a Gaussian distribution and the relative phase between the natural resonance function and the additive noise, ϕ, which is uniformly distributed.

than the multiplet average parameters (A_0, α_0), with α_2 affected the least.

Additive noise biases estimated multiplet parameters, and low NSR should be sought to minimize this effect. However, the most robust signature of large-scale convection is the α_2 coefficient representing the line width variation within a multiplet, which is relatively unaffected by additive noise.

4.3. *Spatial Cross Talk*

Apparent line widths are also affected by the discrete and incomplete spatial sampling of the solar image. If we represent

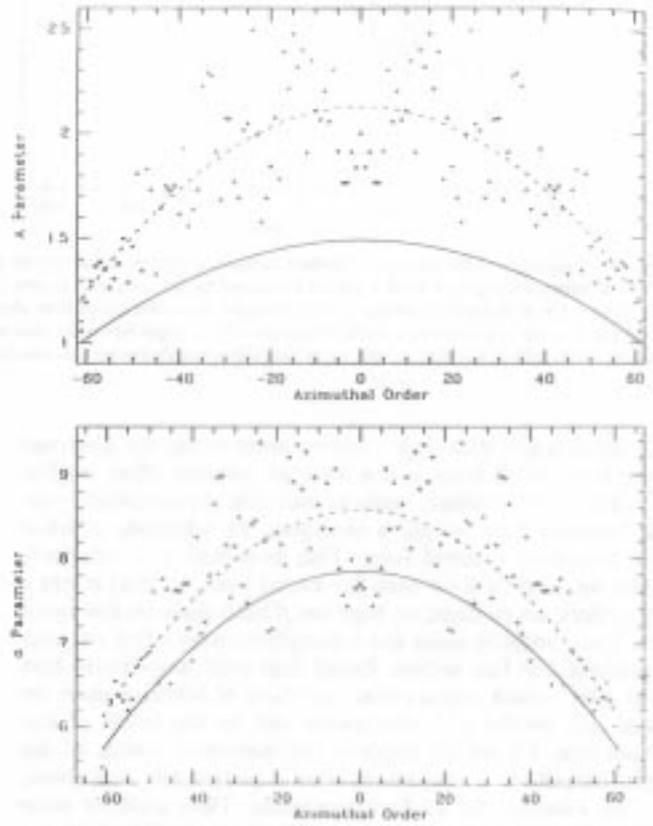

FIG. 10.—Effect of additive noise on the singlet amplitudes and line widths of ${}_3S_{61}$ with power noise-to-signal ratio equal to 15%. *Top:* The input amplitude variation with azimuthal order m is the solid line. Each x marks the average amplitude measurement over 60 realizations of additive noise; they are constrained to be symmetric in m. The dashed line is a degree two Legendre polynomial fit. *Bottom:* same as the top panel, for line widths. On average, additive noise mimics the convective signature on amplitudes and line widths and can be represented simply as a transfer function in m between the input parameters and the measured parameters.

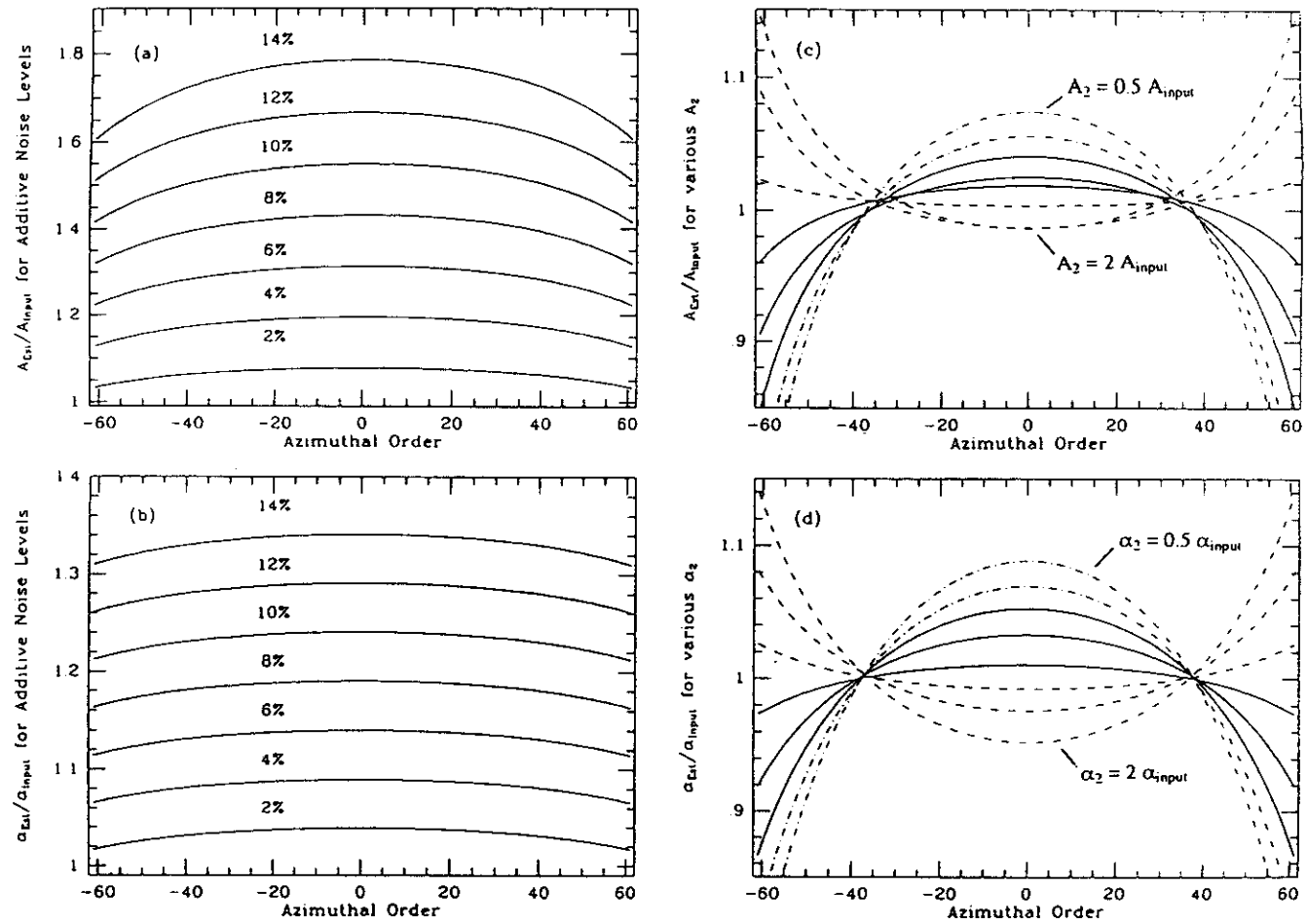

FIG. 11.—Effect of varying the power of the additive noise-to-signal ratio (NSR) and the input multiplet parameters on the transfer function relating the input and measured parameters for ${}_3S_{61}$. Sixty realizations of the additive noise process were performed for each m value. *Left:* (*a*) Transfer function relating input to measured amplitude plotted vs. azimuthal order for seven different values of the NSR: 2%–14% in increments of 2%. (*b*) Same as (*a*), but for line widths α. Comparison of (*a*) with (*b*) shows that line widths are less affected by additive noise than amplitudes, and that the transfer function of line widths may be negligible for small levels of additive noise. *Right:* (*c*) Transfer function relating input to measured amplitude plotted vs. azimuthal order for seven different values of the amplitude trend parameter, A_2, ranging from 0.5 to 2.0 times the input value in uniform increments. (*d*) Same as (*c*), but for line widths ranging from 0.5 to 2.0 times the input value in uniform increments. The dependence of the measured multiplet parameters on the values of the input parameters is weaker than the dependence on NSR, suggesting that for larger values of additive noise, the transfer function might be approximated as being only a function of additive noise level.

the data observed at a single time t as a vector $\mathbf{d}_i(t)$ in which different rows i contain data from the different spatial locations of the solar image, then the data are related formally to their spherical harmonic expansion coefficients c_j by the matrix equation

$$\mathbf{d}(t) = \mathbf{Y}\mathbf{c}(t)\,, \tag{28}$$

where each column of Y represents a unique $\{l, m\}$ combination, and Y_{ij} is the associated spherical harmonic evaluated at the latitude and longitude represented by i. We desire the coefficient time series $c_j(t)$ for spectral analysis, but are typically provided with an approximation, $\hat{c}_j(t)$, that exploits the near orthonormality of the matrix Y,

$$\hat{\mathbf{c}}(t) = \mathbf{Y}^\dagger\mathbf{d}(t)\,, \tag{29}$$

where $\mathbf{Y}^\dagger$ indicates the hermitian transpose of the matrix Y.

The approximate coefficients $\hat{\mathbf{c}}(t)$ can thus be predicted from the desired coefficients $\mathbf{c}(t)$ by substituting equation (29) into equation (28):

$$\hat{\mathbf{c}}(t) = \mathbf{Y}^\dagger\mathbf{Y}\mathbf{c}(t) \tag{30}$$

$$= \mathbf{X}\mathbf{c}(t) \tag{31}$$

Because the solar image is sampled discretely and nonuniformly over a hemisphere, the matrix X contains appreciable off-diagonal elements. These off-diagonal entries are most significant when the sum $l_i + m_i$ for the l and m associated with the ith row has even integral difference from the $l_j + m_j$ sum associated with the jth column. The magnitude of the off-diagonal coefficients is increased with decreasing sampling resolution, or by decreasing the solid angle of the surface observed, for example, by excluding limb data.

Equation (31) can be Fourier transformed to yield

$$\hat{\mathbf{c}}(\omega) = \mathbf{X}\mathbf{c}(\omega)\,, \tag{32}$$

showing that the spectra $\hat{\mathbf{c}}(\omega)$ are typically linear combinations of the spectra we wish to analyze $\mathbf{c}(\omega)$. Thus, a given resonance is contaminated slightly by neighbouring modes, especially those modes within the same multiplet for which $\Delta m = \pm 2$.

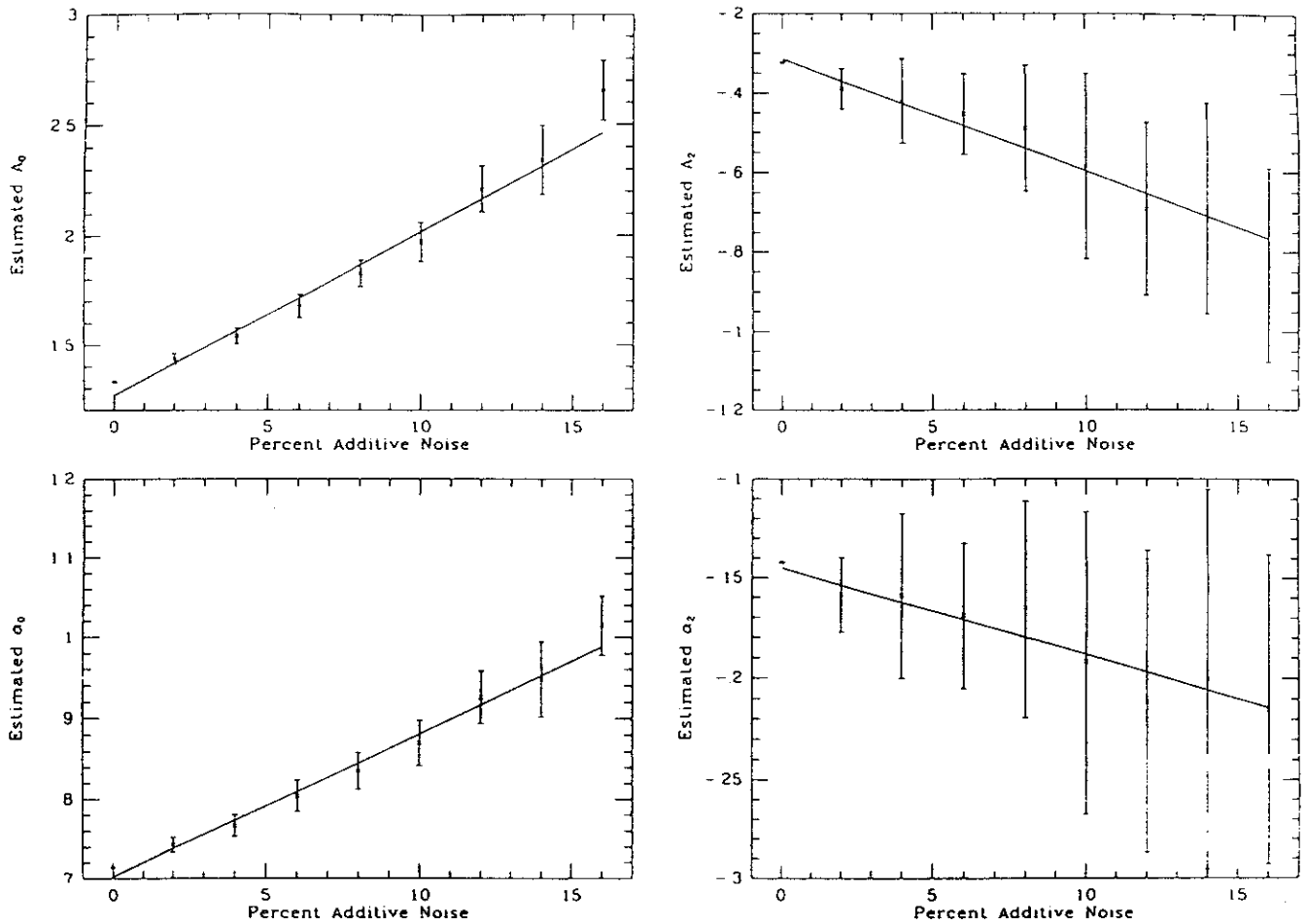

FIG. 12.—Effect of varying the power of the additive noise-to-signal ratio (NSR) on the estimated multiplet coefficients. Sixty realizations of the additive noise were performed at each NSR level. The trend parameters A_2 and α_2 are less affected by additive noise than the apparent degenerate parameters A_0 and α_0, making A_2 and α_2 the more reliable signifiers of large-scale convection.

Since the frequencies of the contaminants are offset from the frequencies of the target mode, cross talk will tend to bias the measured line widths to be too wide.

The magnitude of the bias depends on several factors. As indicated previously, the magnitude of cross talk contamination will depend on the data, and on the image cropping of the data sampling. Measurement bias will also depend upon the size of the intrinsic line width in comparison to the frequency separation of cross talk partners. If the intrinsic line widths are much narrower than the frequency separations, cross talk will produce distinct side lobes that will not affect the measurement of the main lobe's width. If the intrinsic line width is much wider than the separation, the side lobes will be masked within the higher amplitude region of the main lobe, and will produce little effect on line width measurements. The greatest bias should occur when the intrinsic line width is comparable to the frequency separation, $\delta\omega_{\text{cross talk}}$, of cross talk partners, where side lobes merge indistinguishably with the main lobe edges. Thus, we expect that cross talk bias will be maximal at critical intrinsic $Q_c \simeq \omega_0/\delta\omega_{\text{cross talk}}$.

To evaluate the bias due to cross talk, consider the synthetic multiplet ${}_{12}S_{30}$, composed of uniform pure Lorentzians with the line widths and frequencies provided by Lavely & Ritzwoller (1992). Each singlet within the multiplet is given a typical, average line width and amplitude, and subjected to the predicted cross talk that would be produced as a result of using a 100 × 100 observation grid, cropping the image at 90% radius and cosine tapering between 80% and 90% of the solar radius. This experimental configuration was used by T. Brown for his 1989 data set. We then fit each singlet-for its Lorentzian parameters, compute the measured Q for each mode, and plot the ratio of the minimum value Q_{min} to the common input intrinsic value $Q_{\text{intrinsic}}$. Due to the structure of the cross talk matrix, Q_{min} will be given almost always by $Q_{m=0}$, and $Q_{\text{intrinsic}} \simeq Q_{m=1}$. This central line broadening caused by spatial filtering mimics the predicted line broadening signature of convection. Thus, the ratio $Q_{\text{min}}/Q_{\text{intrinsic}}$ provides an estimation of the extent to which Q is reduced by cross talk effects alone.

Figure 13 shows the substantial effect of cross talk on the measured line widths of a uniform multiplet; that is, each singlet within the multiplet has an identical amplitude and line width. We see clearly the sharp bias toward low Q measurements near a critical value of $Q_{\text{intrinsic}} \simeq 2500$, where intrinsic line widths are comparable to the frequency separations of cross talk partners. The magnitude of the bias is significant: cross talk alone can account for a 30% increase in line width, which is smaller than, but of the same order of magnitude of the broadening effect of convection using Glatzmaier's convection model.

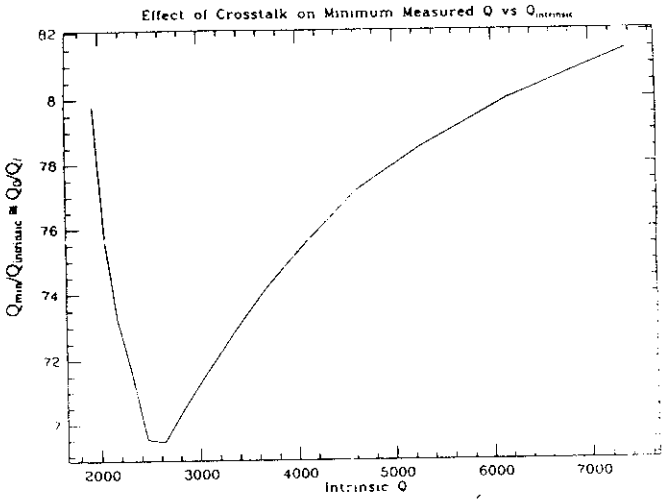

FIG. 13.—Cross talk acts to broaden measured multiplet lines independently of any broadening due to convective coupling. Here, a synthetic multiplet of pure Lorentzian shapes is produced, each singlet having an identical $Q_{\text{intrinsic}} \simeq Q_0$, located at the center frequencies predicted for the multiplet ${}_{12}S_{30}$. The multiplet is then contaminated by the predicted cross talk that would result for an observed solar image sampled on a 100 × 100 grid cropped at 0.9 solar radii. Each singlet is then least-squares fitted individually for Lorentzian parameters. The ratio of the minimum Q measurement (normally Q_0) among these generalized resonance functions to its input intrinsic value is plotted as a function of the input $Q_{\text{intrinsic}}$. A minimum occurs near $Q_{\text{intrinsic}} \simeq 2500$, where cross talk sidelobes merge to the edges of the main lobe. This effect competes with broadening due convective coupling, but can be ameliorated using the technique of singlet stripping.

This bias due to cross talk can be substantially reduced using the technique of *singlet stripping* (Ritzwoller, Masters, & Gilbert 1986). Recall from equation (32) that we know the relation between the desired, cross talk–free spectra $c(\omega)$, and the observed spectra $\hat{c}(\omega)$. The matrix relating the two, X, is easily computable, and depends only on the observational setup. We can thus formally invert equation (32) to obtain

$$c(\omega) = X^{-1}\hat{c}(\omega) . \tag{33}$$

In principle, this technique could be used to strip both intra and intermultiplet cross talk from the data by including every (l, m) combination as a row in $\hat{c}$. For our purposes, however, it will suffice to consider a multiplet at a time, and limit the rows of $\hat{c}$ to include only spectra within that multiplet. This approximation will completely remove cross talk from within the multiplet, thus eliminating the cross talk from resonances having azimuthal order difference ($\Delta m = \pm 2$), which are the dominant contributors to line width measurement bias. A substantial cross talk contribution from neighboring modes having $\Delta l = \pm 1$ and $\Delta m = \pm 1$ cannot be removed, because the strong similarity of the spatial shapes of these modes produces a cross talk matrix with very similar columns, and such matrices are very unstable to inversion. Inversion stability can be measured by the condition number, which is the ratio of the largest to smallest singular values of the cross talk matrix's singular value decomposition. When single multiplets alone are considered the condition number is typically $\mathcal{O}(10)$, if there is sufficient spatial sampling for the harmonic degree of the multiplet. This will generally be the case if $n_{\text{grid}} \geq l$, where n_{grid} is the number of grid points along an edge of the solar image. When neighboring multiplets are considered, however, the condition number becomes typically $\mathcal{O}(10^4)$. Such matrices are very sensitive to noise and round-off error, and cannot be inverted reliably.

The cross talk component from neighboring multiplets will not directly affect line width measurements, however, since the frequency separation between the main resonance peak and the cross-multiplet cross talk is always many times larger than the resonance line widths for multiplets of interest. The cross talk–to–main-peak frequency separation may be approximately 11.6 μHz for these multiplets, however, which will allow the day–night side lobes of the cross talk peak to overlap the main peak and bias measurements made on its line width. Knowing the time history of the observation window would allow us to compute the strength of these side lobes and incorporate this effect into forward models, but removing this effect from observational data is very difficult. This problem should be overcome when continuous data become available from the GONG network, which will enable us to produce spectra having minimal side lobes.

To test this singlet stripping technique, we prepared synthetic spectra for multiplet ${}_{14}S_{20}$ having the expected line width patterns, and subjected it to the cross talk produced by a 100 × 100 grid cropped at 85% of image radius. We found that singlet stripping removes perfectly the bias induced by cross talk. The technique is limited only by the inversion stability of the matrix X, which depends only on the experimental setup and on the harmonic degree of the multiplet to which the singlet stripping is applied. The matrix inversion is unstable if there are too few grid points in the image to adequately differentiate between Y_{lm} functions within a multiplet. We can ensure such sufficient resolution by limiting the use of singlet stripping to multiplet of harmonic order l less than the number of grid points across one edge of the image. The matrix inversion will also become unstable if too many limb data are rejected, as would occur if the image is cropped below 80% of its radius.

5. DISCUSSION AND CONCLUSIONS

This is part of a series of papers (Ritzwoller & Lavely 1991; Lavely & Ritzwoller 1992, 1993; and Ritzwoller & Kelly 1993) which addresses the effect of large-scale convection on helioseismic oscillations. This paper is the first to discuss methods by which the convective line width signature predicted by Lavely & Ritzwoller (1993) can be observed in helioseismic data which are modified by a stochastic source spectrum. The goal of these studies is to provide the background necessary to establish clearly the existence of giant cell convection in the deep solar interior and, once established, to constrain the statistical characteristics of its nature, perhaps as a function of time over a solar cycle.

Our goal here has not been to present the optimal technique for recovering line shape information in helioseismic data, but rather to present evidence for the existence of one such technique. With this "existence proof" we encourage observers to turn toward a greater interest in modal line widths and amplitudes. Recovery of information about natural line shapes will require the continuing development of intelligent new methods of data analysis, but promises to reveal nonaxisymmetric structures which may hold the key to a greater understanding of solar dynamics rather than the purely structural information dominantly revealed by modal frequencies.

To detect the line-broadening signature of large-scale convection, time series should be as long and as ungapped as practically possible. Long/ungapped time series have the positive effect of minimizing the width of the convolution filter in

the frequency domain which can obscure the natural line widths. In addition, the signal to additive noise ratio increases with time series length. Thus, longer time series reduce the line width bias introduced by additive noise. These considerations underscore the need for the use of Global Oscillations Network Group (GONG) data and space-based measurements, such as those expected from the *Solar Orbiting Heliospheric Observatory (SOHO)*.

In closing, we summarize the conclusions we have drawn.

1. A method to retrieve natural line width information beneath a stochastic source spectrum has been presented. The recommended method, represented by equations (10) and (20)–(24), is called quasi–Monte Carlo spectral parameter estimation.

2. Application of this method to a single multiplet results in estimates that converge to a pure Lorentzian fit. Unfortunately, such estimates are biased by the deviation of the source spectrum for this multiplet from an "average" source spectrum.

3. Error estimates produced by Monte Carlo source spectrum modeling adequately represent these biases.

4. Although these equations are applied to retrieve line width parameters for a single multiplet, to estimate accurately the natural line width signature predicted by Lavely & Ritzwoller (1993) requires the inclusion of information from more than a single multiplet. In particular, line width variations along a dispersion branch can be accurately retrieved.

5. Quasi–Monte Carlo parameter estimation encompassing lines from more than a single multiplet will produce results superior to those presented here, although they will be more computationally costly.

6. Even neglecting the effects of modal cross talk and additive noise, time series lengths in excess of 20 days are required to retrieve the input line width signal. Day–night gaps are less important than overall time series lengths with respect to line width estimation accuracy.

7. Additive noise tends to accentuate the signature of large-scale convection and biases estimates of the multiplet parameters. Fortunately, the least sensitive parameter to the effect of additive noise is the line width variation parameter, α_2, which is the most robust signature of convection. Nevertheless, observers should seek high signal-to-noise modes to minimize this effect.

8. Cross talk produces a significant bias in the estimation of line widths tending to broaden their measured values similarly to the predicted broadening due to giant cell convection. If giant cell convection is to be unambiguously observed in line width patterns, it will almost certainly be necessary to correct for cross talk using the technique of singlet stripping or other similar methods, until higher resolution data becomes available.

9. Observers should concentrate on observing and interpreting line width variations within and across multiplets to discern the helioseismic effect of large-scale convention.

We thank Timothy Brown and Eugene Lavely for valuable conversations. This work was supported by the National Science Foundation under grant ATM-91-22571. Parts of this research were performed at the National Center for Supercomputing Applications at the University of Illinois, Urbana-Champaign.

REFERENCES

Anderson, E. 1993, GONG 1992: Seismic Investigation of the Sun and Stars, ed. T. M. Brown (ASP Conf. Ser., 42, 445)
Brown, T. M. 1990, ApJ, 371, 396
Chao, B. F., & Gilbert, F. 1980, Geophys. JRAS, 63, 641
Dahlen, F. A. 1979, Geophys. JRAS, 58, 1
Dziewonski, A. M., & Woodhouse, J. H. 1983, Proc. Enrico Fermi Sch. Phys., Vol. 85, ed. H. Kanamori & E. Boshi, Earthquakes: Observation, Theory & Interpretation (North-Holland: Elsevier), 45
Gilman, P. A., & Glatzmaier, G. A. 1981, ApJ, 45, 335
Gilman, P. A., & Miller, J. 1986, ApJS, 61, 585
Glatzmaier, G. A. 1984 J. Comp. Phys., 55, 461
Glatzmaier, G. A., & Gilman, P. A. 1981, ApJS, 45, 351
———. 1982, ApJ, 256, 316
Goldreich, P., & Kumar, P. 1988, ApJ, 326, 462
Goode, P. R., Dziembowski, W. A., Korzennik, S. G., & Rhodes, E. H. 1991, ApJ, 367, 649
Kumar, P., & Goldreich, P. 1989, ApJ, 342, 558
Lavely, E. M., & Ritzwoller, M. H. 1992, Phil. Trans. R. Soc. Lond., A, 339, 431
———. 1993, ApJ, 403, 571
Lindberg, C. R., & Park, J. 1987, Geophys. JRAS, 91, 795
Masters, G., & Gilbert, F. 1983, Phil. Trans. R. Soc. Lond., A308, 479
Park, J., Lindberg, C. R., & Thomson, D. J. 1987, Geophys. JRAS, 91, 755
Ritzwoller, M. H., Masters, G., & Gilbert, F. 1986, J. Geophys. Rev., 91, 10203
Ritzwoller, M. H., & Kelly, J. F. 1993, GONG 1992: Seismic Investigation of the Sun and Stars, ed. T. M. Brown (ASP Conf. Ser., 42, 261)
Ritzwoller, M. H., & Lavely, E. M. 1991, ApJ, 369, 557
Woodard, M. 1984, in Ph.D. thesis, University of California, San Diego